nature sustainability

Article

https://doi.org/10.1038/s41893-022-00977-7

Large and inequitable flood risks in Los Angeles, California

Received: 6 April 2022

Accepted: 12 September 2022

Published online: 31 October 2022

Check for updates

Brett F. Sanders[1,2,3] ✉, Jochen E. Schubert[1,3], Daniel T. Kahl[1], Katharine J. Mach[4,5], David Brady[6,7], Amir AghaKouchak[1,3,8], Fonna Forman[9,10], Richard A. Matthew[2,3], Nicola Ulibarri[2,3] and Steven J. Davis[1,3,8]

Flood risks in the United States have historically been underestimated, particularly with respect to human well-being and within low-wealth and marginalized communities. Here, we characterize a fuller range of risks in Los Angeles, California, using a quantitative framework that intersects flood hazards from rainfall, streamflow and storm tides with measures of exposure and vulnerability including ethnicity, race and socioeconomic disadvantage. We find that between 197,000 and 874,000 people (median 425,000) and between US$36 billion and US$108 billion in property (median US$56 billion) are exposed to flooding greater than 30 cm within the 100-year flood zone, risk levels far above federally defined floodplains and similar to the most damaging hurricanes in US history. These risks are disproportionately higher for non-Hispanic Black and disadvantaged populations, burdening communities that may have greater challenges recovering and reinforcing socioeconomic inequities. Our framework creates opportunities for transparently and equitably reducing flood risks in urban areas.

Flood damages and the frequency of billion-dollar flooding disasters are on the rise in the United States[1], especially in urban areas[2,3] due to the combined effects of increasing development in flood zones[4] and more intense precipitation and runoff from global warming and urbanization[5,6]. Floods damage property and infrastructure, disrupt economic activity, displace people, harm communities and degrade ecosystems[3,7]. As with other environmental impacts[8,9], flood damages are not evenly distributed across social and demographic groups. In particular, poor and non-white populations have been disproportionately affected and less well protected[10–12]. Such inequities are critically important because recovery from floods is often prolonged and incomplete among socially marginalized, low-wealth and vulnerable communities, also due to unequal support in flood risk reduction and disaster recovery by governments, all of which serves to compound and reinforce the inequities[13].

Worldwide, the costliest flood disasters have been related to US hurricanes (tropical cyclones): the top six events all occurred in the United States and accounted for losses of >US$50 billion each[1,14]. Hurricanes have also accounted for 60% of all flood-related population displacements in the United States since 1985 (ref. [15]). This has drawn considerable attention to hurricane risks facing cities along the coasts of the Gulf of Mexico and Eastern seaboard where populations are

[1]Department of Civil and Environmental Engineering, University of California, Irvine, CA, USA. [2]Department of Urban Planning and Public Policy, University of California, Irvine, CA, USA. [3]UCI Blum Center for Poverty Alleviation, University of California, Irvine, CA, USA. [4]Department of Environmental Science and Policy, Rosenstiel School of Marine, Atmospheric, and Earth Science, University of Miami, Miami, FL, USA. [5]Leonard and Jayne Abess Center for Ecosystem Science and Policy, University of Miami, Coral Gables, FL, USA. [6]School of Public Policy, University of California, Riverside, CA, USA. [7]Blum Initiative on Global and Regional Poverty, University of California, Riverside, CA, USA. [8]Department of Earth System Science, University of California, Irvine, CA, USA. [9]Department of Political Science, University of California, San Diego, CA, USA. [10]Center for Global Justice, University of California, San Diego, CA, USA. ✉e-mail: bsanders@uci.edu

concentrated, as well as more rural areas in the Southeast where high hazards and high vulnerabilities align[12,16]. Although cities along the West Coast rarely experience hurricanes, severe flooding from heavy rainfall caused losses >US$1 billion in both 2017 and 2021 (ref. [1]), pointing to the risks of catastrophic flooding from severe atmospheric river events[17,18].

The most notable recorded atmospheric river event in the United States was the Great Flood of 1861–62, which caused a catastrophe in California with major impacts to the fishing, ranching and mining industries—the economic engines of the state at that time[19]. One-third of taxable properties were destroyed, which bankrupted the state, and deep flooding of Sacramento forced the temporary relocation of the state government to San Francisco. The atmospheric event was characterized by a return period of 500–1,000 years and flooding of Los Angeles was characterized by a return period of 500 years (ref. [17]). The Los Angeles region was then mostly ranchlands with fewer than 15,000 residents and after 4 weeks of rain punctuated by more than a day of intense rainfall, losses were marked by ~200,000 cattle, ~100,000 sheep and ~500,000 lambs[19]. Today, a population of 10 million people[20] and a US$748 billion-per-year economy[21] occupy Los Angeles County, reliant on a network of dams, levees and drainage channels for protection[22].

The ARkStorm study led by the US Geological Survey (USGS) contemplated the possibility of the Great Flood occurring in present-day California, impacting the largest statewide economy and population of the United States[17]. The study concluded that the existing flood control infrastructure was undersized and flooding would resemble what occurred before infrastructure was in place[19]. Economic losses were estimated at over US$700 billion, which far exceeded damages of climate-related disasters in recorded history (for example, ref. [14]). In a state that has adapted to earthquake risk with increased awareness and the retrofit and upgrade of many structures, the project aimed to increase flood risk awareness and stimulate risk reduction measures. Unfortunately, the risk assessment had little traction with public works and emergency managers who expressed confidence in infrastructure for protection[19]. Roughly a decade earlier, over US$200 million had been spent to raise levees and construct flood walls along the Rio Hondo Channel and lower Los Angeles River (Supplementary Fig. 1) to contain a 100-year return period event (ref. [22], page 151).

Today, the most recent Federal Emergency Management Agency (FEMA) flood hazard maps for Los Angeles County (Supplementary Fig. 1) show a very small '1% annual chance flood hazard' area with a population of only 23,169, or <0.3% of the population, where flood insurance is required under the National Flood Insurance Program. This exposure is reflective of fluvial and coastal flooding only, in line with FEMA directives for flood hazard mapping[23], so pluvial flood hazards have not been addressed. Moreover, areas defended by the newly raised levees and flood walls fall within an 'area with reduced risk due to levee' that contains a population of 287,235 (based on 2020 census) and where flood insurance is not required to limit financial burdens on exposed populations—a motivating factor for the levee project (ref. [22], page 149). However, FEMA flood maps that underestimate risks have been well documented across the United States[24], flood peaks have continued to increase from urbanization across Los Angeles County[25] and recent reports by the US Army Corps of Engineers and Los Angeles County Department of Public Works reveal that segments of the Los Angeles River, Dominguez Channel, Compton Creek and San Gabriel River (Fig. 1a) are either undersized to contain a 100-year flood peak[26,27] or in unacceptable condition for flood protection because of in-channel sedimentation, vegetation growth, spalling of concrete and gaps in flood walls[28]. Furthermore, the region's major dams are in poor condition. On the basis of the US Army Corps of Engineers Dam Safety Action Classification for risk assessment[29], one major dam has been classified at the highest level of concern, 'urgent and compelling', and several more at the second highest level, 'urgent' (Supplementary Fig. 1). Collectively, these factors indicate that a 100-year flood event in Los Angeles will not be contained by existing infrastructure, which points to a high disaster risk and calls for a more detailed risk assessment, including the number of people and amount of property exposed, the capacity of the population to recover, hot spots of exposure and socioeconomic and racial inequities in exposure.

Here, we present an innovative framework to reveal the magnitude and inequity of flood exposure in Los Angeles at countywide and municipal scales. Improved risk awareness is crucial for protecting lives and livelihoods and for planning and designing cost-effective and equitable flood adaptation measures. The details of our analysis framework are described in the Methods. In summary, we use a statistical and hydrodynamic model[30] to map inundation and flood hazards at 3 m resolution across Los Angeles County (Fig. 1a), a level of detail that captures patterns of street flooding from intense precipitation (Fig. 1c) and from excess streamflow that cannot be contained by major drainage channels (Fig. 1d,e). Using an extensive set of local gauge data, flooding from precipitation, streamflow and coastal storm tides (Fig. 1f–h) is evaluated separately for a canonical 100-year return period event estimated at the 5th, 50th and 95th percentile (to capture uncertainty) and we then analyse composite and driver-specific flood risks at the parcel level on the basis of parcel land use and property value[31] and block-group-level estimates of income, race and ethnicity[32]. We also evaluate these risks according to indicators of census-tract-level social vulnerability (the national social vulnerability index, SoVI) and a higher-resolution assessment of neighbourhood disadvantage (the neighbourhood disadvantage index, NDI) based on block-group-level data from the American Community Survey[32] (Methods).

Results

The composite 100-year flood zone for Los Angeles, the overall flood zone accounting for pluvial, fluvial and coastal hazards, exposes a population of 1.3–2.4 million people (5th–95th percentile, median 1.7 miliion) and US$215 billion–US$346 billion in property (median US$265 billion) to flooding >3 cm and 197,000–874,000 people (median 425,000) and US$36 billion–US$108 billion in property (median US$56 billion) to flooding >30 cm (Fig. 1b and Supplementary Table 1). Flooding deeper than 3 cm is mainly related to pluvial hazards (1.2 million–1.8 million people, Fig. 1f) and fluvial hazards (81,000–1.1 million, Fig. 1g), which are much more widespread than coastal hazards (4,000–7,000, Fig. 1h). Flooding >100 cm, on the other hand, is mainly related to fluvial hazards (3,000–323,000 people, median 83,000) with a smaller contribution from pluvial hazards (31,000–58,000 people, median 40,000), occurring when primary drainage channels are unable to contain flood flows (compare ref. [19]).

Flood exposure representativeness (FER) is the fraction of a population by race or ethnicity living in the flood zone divided by the fraction of the same group within the region[33] and differences in FER from unity indicate inequities in exposed populations. With the flood zone for Los Angeles evaluated at the 50th percentile, non-Hispanic Black and Hispanic residents are disproportionately exposed to flood risks based on FER of 1.24 and 1.06 and flood depths >3 cm, respectively, while non-Hispanic Asian and non-Hispanic White residents are disproportionately less exposed based on FER of 0.92 and 0.93, respectively. Given the ratio of FER values, non-Hispanic Black and Hispanic residents are thus 31% and 13% more likely than non-Hispanic White residents to be exposed to flooding >3 cm. Moreover, non-Hispanic Black, Hispanic and non-Hispanic Asian residents are 79% (FER = 1.62), 17% (FER = 1.00) and 11% (FER = 0.94) more likely than non-Hispanic White residents (FER = 0.83) to be exposed to deep flooding (>100 cm).

Lorenz curves offer an integrated measure of flood risk inequity by comparing the cumulative distribution of flood depth with cumulative population sorted by a particular factor (for example, property value, income, disadvantage and race). Flood hazards equally distributed across the population would plot along a 1:1 line and any deviations reflect inequalities that, when integrated, are a quantitative indicator: the Gini coefficient[34] (G).

https://doi.org/10.1038/s41893-022-00977-7

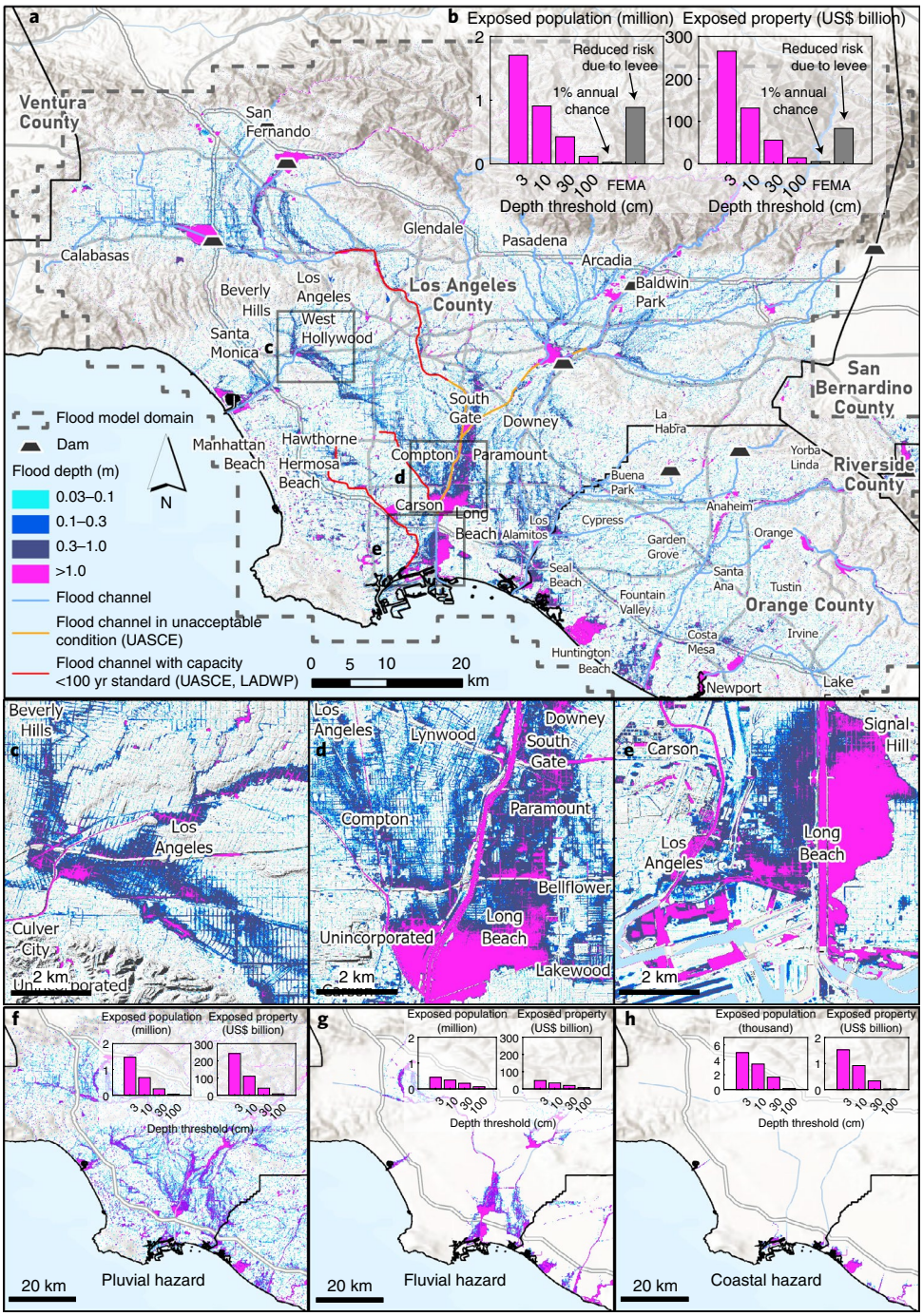

Fig. 1 | 100-year compound flood hazard in Los Angeles. a, Spatial distribution of simulated 100-year composite flood hazard depth evaluated at the 50th percentile and condition of major flood channels with respect to containing a 100-year flood event. **b**, Exposed population (in millions) and exposed property (in US$ billions) for several depth thresholds far exceeds population within FEMA 1% annual chance flood zone. **c**–**e**, Magnified view of pluvial flooding in the west side of Los Angeles County (**c**), compound fluvial–pluvial in the south central part of Los Angeles County (**d**) and compound fluvial–coastal flooding near Long Beach (**e**) shows the street-level detail resolved by the modelling framework. **f**–**h**, Spatial distributions of hazard and exposure corresponding to pluvial flooding (**d**), fluvial flooding (**e**) and coastal flooding (**e**) show that deep flooding (30–100 cm) is driven by fluvial and pluvial hazards and widespread shallow flooding (3–10 cm) is driven by pluvial hazard. Note that coastal population exposure is in thousands. Basemaps in **a** and **c**–**h** are from World Terrain Base[63].

The Lorenz curve of the composite 100-year flood hazard evaluated at the 50th percentile (Fig. 2a, Supplementary Fig. 2 and Supplementary Table 2) shows the strongest disproportionality when population is sorted by the share of Black population ($G = 0.32$), driven mainly by fluvial ($G = 0.51$) and pluvial flood hazards ($G = 0.12$). Figure 2b shows that areas near Carson have the highest shares of non-Hispanic Black population and high flood hazard (Fig. 1a,d). In contrast, non-Hispanic White populations are disproportionately less exposed to the composite flood hazard ($G = -0.23$) and especially fluvial hazards ($G = -0.33$). This is consistent with low shares of non-Hispanic White populations living in the high flood hazard region between Carson and South Gate (Fig. 2e). Hispanic populations are also somewhat disproportionately exposed to the composite ($G = 0.07$) and fluvial flood hazards ($G = 0.12$), consistent with the prevalence of

https://doi.org/10.1038/s41893-022-00977-7

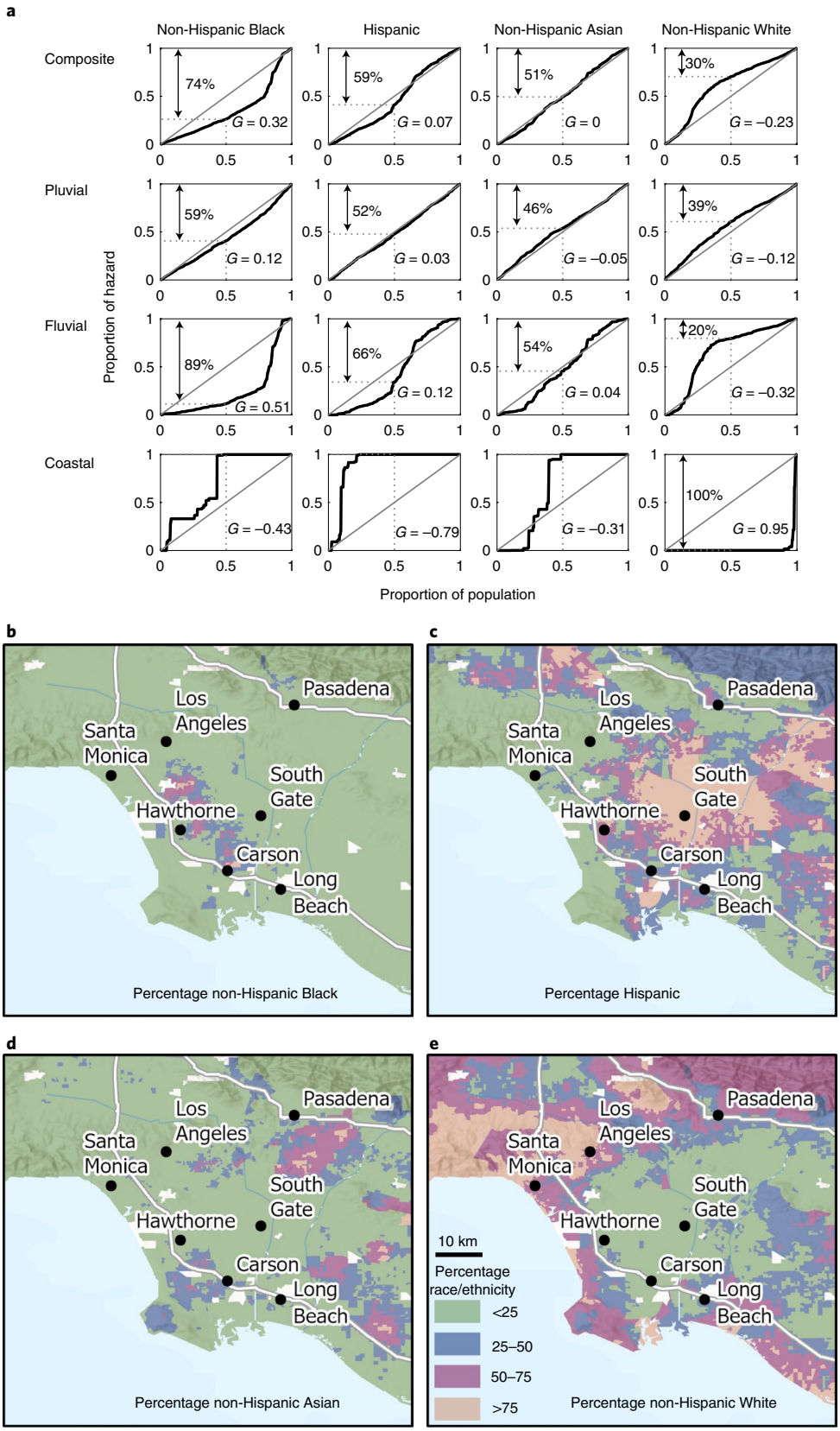

Fig. 2 | Flood exposure by race and ethnicity. a, Lorenz curves of population-weighted flood hazard with Gini coefficients (*G*) for the 100-year return period composite hazard, pluvial hazard, fluvial hazard and coastal hazard evaluated at the 50th percentile and four racial/ethnic sorting variables. **b**–**e**, Maps showing non-Hispanic Black population fraction (**b**), Hispanic population fraction (**c**), non-Hispanic Asian population fraction (**d**) and non-Hispanic White population fraction (**e**). Gini coefficients show that fluvial flood hazards disproportionately impact non-Hispanic Black populations ($G = 0.51$) and Hispanic populations ($G = 0.12$), pluvial flood hazards disproportionately impact non-Hispanic Black populations ($G = 0.12$) and coastal hazards almost exclusively impact non-Hispanic White populations ($G = 0.95$). Percentages reflect the fraction of the hazard associated with the upper half of the population by the sorting variable. See Fig. 3b for population density. Basemaps in **b**–**e** from World Terrain Base[63].

https://doi.org/10.1038/s41893-022-00977-7

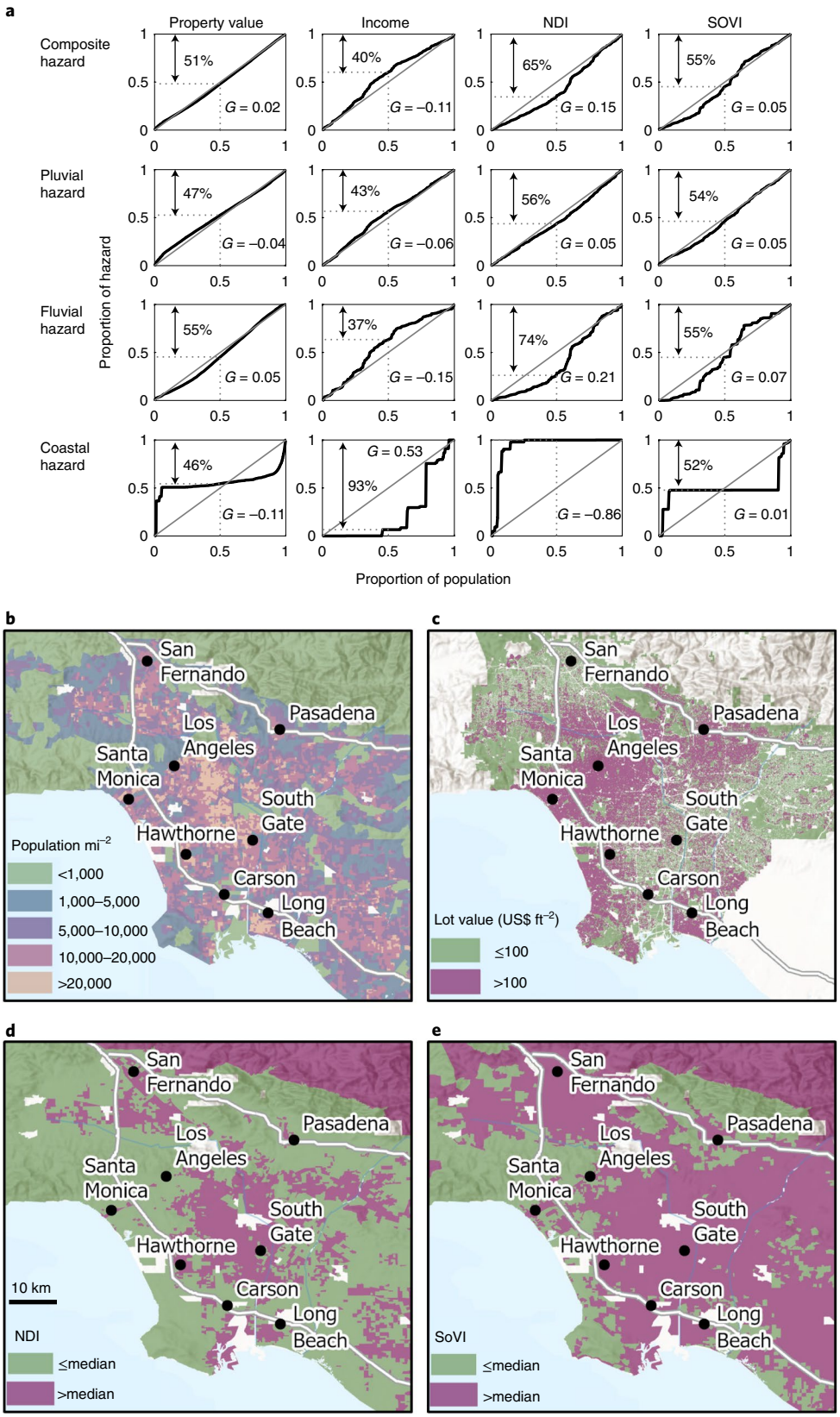

Fig. 3 | Flood exposure by socioeconomic indicators. a, Lorenz curves of population-weighted flood hazard with Gini coefficients (*G*), for the 100-year return period composite hazard, pluvial hazard, fluvial hazard and coastal hazard evaluated at the 50th percentile and four different sorting variables. **b**, Block-group-scale population density used for dasymetric estimation of population at the parcel scale. **c**–**e**, Maps showing: property value, income (**c**), neighbourhood disadvantage (**d**) and the SoVI (**e**). Percentages reflect the fraction of the hazard associated with the upper half of the population by the sorting variable and show that exposure does not differ by property value, that more disadvantaged populations are disproportionately exposed to the composite hazard ($G = 0.15$), driven by fluvial flood hazards ($G = 0.21$) and that less disadvantaged populations are almost exclusively exposed to coastal hazards ($G = -0.86$). Basemaps in **b**–**e** from World Terrain Base[63].

https://doi.org/10.1038/s41893-022-00977-7

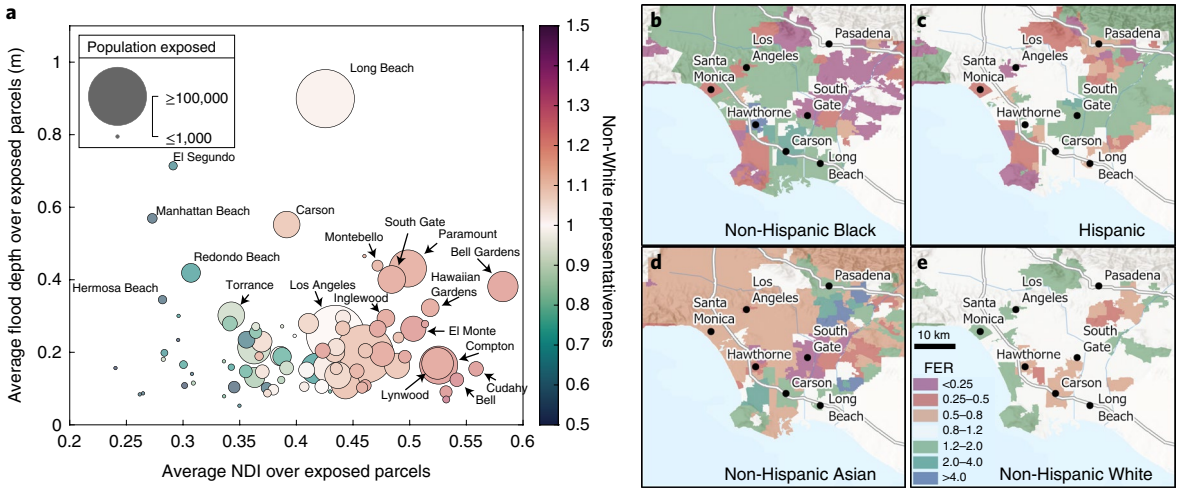

Fig. 4 | Prioritization of risk reduction resources. a, Aggregation of parcel-level data at municipal levels, considering exposed population (bubble size), flood hazard (*y* axis) and disadvantage (*x* axis). This multidimensional assessment of risk presents three complementary, non-racial factors deserving of consideration for prioritization of risk reduction resources. Non-White representativeness is the fraction of the non-White population in the flood zone relative to the same fraction in the region. **b**–**e**, Prioritization could also consider inequities across racialized groups indicated by FER at municipal levels for non-Hispanic Black (**b**), Hispanic (**c**), non-Hispanic Asian (**d**) and non-Hispanic White populations (**e**). Basemaps in **b**–**e** are from World Terrain Base[63].

Hispanic populations in the high hazard region surrounding South Gate (Fig. 2c). Meanwhile, there is little indication of inequality in the exposure of non-Hispanic Asian populations to the composite hazard ($G = 0.00$; Fig. 2d) and almost only non-Hispanic White populations are exposed to coastal hazards ($G = 0.95$; Fig. 2e).

Despite the racial inequalities, our results suggest that extreme flooding in Los Angeles would not discriminate by property value. Lorenz curves for the composite hazard sorted with respect to property value (Fig. 3a, Supplementary Fig. 2 and Supplementary Table 2) closely track the line of perfect equality ($G = 0.02$), which is consistent with a mix of lower-than-median and higher-than-median property values within the main flood hazard corridor near South Gate and Carson (Fig. 3c). However, there are modest disproportionalities with respect to income ($G = -0.11$) and disadvantage as measured by NDI ($G = 0.15$) and a weak disproportionality with respect to vulnerability as measured by SoVI ($G = 0.05$). The main flood hazard corridor is associated with higher-than-median SoVI (Fig. 3e) and both higher-than-median and lower-than-median NDI (Fig. 3d), with higher SoVI and NDI values indicative of higher social vulnerability and neighbourhood disadvantage, respectively. More disadvantaged populations will face greater challenges recovering from floods and Lorenz curves show that the more disadvantaged half of the population shoulders 65% of the composite flood hazard, 56% of the pluvial flood hazard and 74% of the fluvial hazard but <1% of the coastal flood hazard.

In the United States, addressing flood risk begins with local government and requires regional, state and federal coordination. The demands of grant writing within a complex application process has led to greater success among more affluent municipalities in securing resources to address flooding[35,36] and, conversely, less success for more disadvantaged communities. Our multidimensional modelling framework at the region scale supports identification of the most at-risk communities considering flood hazard severity, population exposed and disadvantage, which can be used to prioritize resource allocations more equitably and transparently. For example, Fig. 4a shows the relationship of disadvantage and flood hazard aggregated to the level of municipalities in the study area and reveals the relatively few cities where both disadvantage and flood risks are high. Among these doubly at-risk municipalities, the most populous are Long Beach, Paramount, Carson, Bell Gardens and South Gate. At a high level, our results suggest that these communities might be worthy priorities for mitigating regional flood risks. In each case, these municipalities are also home to a substantial share of non-white residents. Increasing hazard and increasing disadvantage represent complementary, non-racialized considerations for prioritizing risk reduction resources on the basis of the magnitude of risks and the capacity of communities to recover, respectively. Furthermore, prioritization of resources could help to address racial disparities by additionally considering where non-white representativeness is high (Fig. 4a–e). For example: Long Beach has an exposed population of 88,000–262,000 (median 208,000) people that is disproportionately non-Hispanic Black (FER = 1.67, Fig. 4b); Paramount has an exposed population of 15,000–53,000 (median 41,000) people that is disproportionately non-Hispanic Black (FER = 1.61) and Hispanic (FER = 1.61); Carson has an exposed population of 17,000–46,000 (median 21,000) people that is disproportionately non-Hispanic Black (FER = 3.27, Fig. 4b); Bell Gardens has an exposed population of 25,000–30,000 (median 28,000) people that is disproportionately Hispanic (FER = 1.98); and South Gate has an exposed population of 13,000–29,000 (median 23,000) people that is disproportionately Hispanic (FER = 1.89, Fig. 4c). The largest municipal exposure corresponds to Los Angeles (514,000–882,000, median 654,000) with an average flood depth of 25 cm and disproportionate exposure of non-Hispanic Black populations (FER = 1.38, Fig. 4b).

Discussion

A 100-year flood event in Los Angles would expose 197,000–874,000 (median 425,000) people and US$36 billion–US$108 billion (median US$56 billion) in property to flooding >30 cm, rivalling the impacts of recent severe US hurricanes such as Katrina in 2005, Sandy in 2012 and Irma and Harvey in 2017, each of which incurred losses >US$50 billion[14] and displaced >200,000 people[15]. The risks of deep flooding (>100 cm) marked by an exposed population of 32,000–361,000 (median 119,000) and exposed property valued at US$7 billion–US$41 billion (median US$14 billion) are primarily linked to overtopping of flood channels mostly constructed in the decades following World War II[22,37] and now undersized[26,27] or inadequately maintained[28]. Precipitation and streamflow records were not widely available during the time of their construction and channel capacity has been reduced over time by sedimentation and in-channel vegetation[37] while runoff rates have increased due to the expansion of impervious surfaces[25]. Our results

https://doi.org/10.1038/s41893-022-00977-7

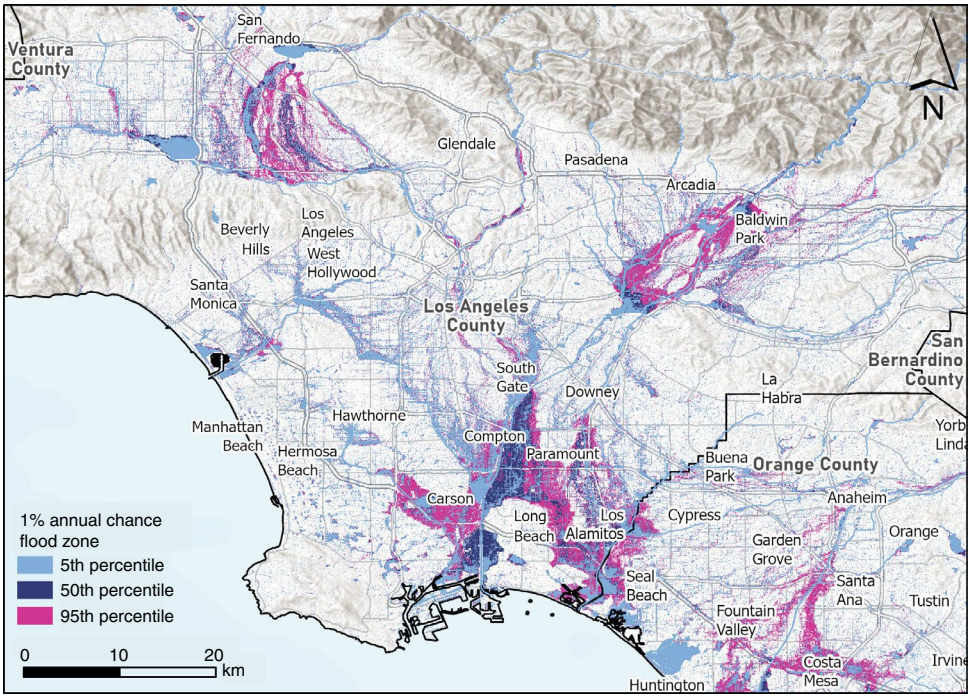

Fig. 5 | Uncertainty in the 100-year return period flood hazard area. Estimated spatial extent of the 100-year return period (1% annual chance) flood hazard zone corresponding to the 5th, 50th and 95th percentiles for uncertainty. In areas of overlap, the lowest percentile is shown. Basemap from World Terrain Base[63].

show that overtopping of upslope channels distributes flood waters over the wide coastal plain, where they flow downslope along roadways and collect within the lowlands between South Gate and Long Beach (where braided channels, riparian wetlands and coastal marsh existed before human development) (ref. [22], page 21).

Flooding causes many types of harms: direct financial losses, property damage, mortality and other impacts to health and well-being, involuntary displacement and transportation and livelihood disruptions, among others[38]. These impacts, in combination with differential vulnerability and coping capacity, can heighten existing inequalities, reduce funds available for governments for other social goods and erode connections to places and the vitality and cohesion of communities. Further, in many cases, flood management practices have served to exacerbate social, economic and political inequities, leading to both differential flood risks and differential relief and recovery following flood disasters[11,39–42].

Models used for continental- and global-scale estimates of flood risk rely on a priori estimates of the level of protection provided by infrastructure (for example, exceedance probability) and assume that fluvial flooding does not occur for flow rates below the protection standard (for example, refs. [23,43]). If FEMA levee ratings are the basis for protection standards used in large-scale models, this may explain why recent nationwide studies (for example, refs. [12,24],) point to much lower risks to Los Angeles than we do. Indeed, urban flood risks in the United States may be systematically underestimated in this way, which could help explain the high frequency of flooding disasters in major US cities[2]. But our results for Los Angeles show that the high-resolution compound flood hazard modelling framework presented here, free from a priori assumptions about channel capacity, can yield exposure assessments that are consistent with detailed studies at the local level (for example, refs. [25,26]) documenting undersized or inadequately maintained channels while systematically characterizing impacts region wide.

Underestimation of urban flood hazards in the United States may limit understanding of inequities in flood exposure. For example, nationwide flood modelling has suggested that non-Hispanic White populations are disproportionately exposed to flood risks at present, partly reflecting exposures concentrated in the Southeastern United States[12,16]. Flood hazards are also perceived and prioritized differently and, for coastal flooding in particular, amenity values may lead to overvaluation of property values, in combination with underestimation of flood risks (for example, ref. [44]). However, our compound hazard modelling in Los Angeles vindicates the experiences of flood management that there are substantial racial and socioeconomic disparities in flood risks by hazard driver. Non-Hispanic Black, Hispanic and socioeconomically vulnerable populations in Los Angeles are disproportionately at risk of fluvial flooding, whereas risks of coastal flooding overwhelmingly pertain to non-Hispanic White and low-disadvantage populations. Our results thus provide an evidentiary basis for understanding unequal distributions of flood risks across communities and demographic groups. As has been found in analyses of exposure to environmental contaminants[9], inequities in flood risks among non-Hispanic Black populations (Fig. 2) seem substantially larger than inequities across levels of neighbourhood disadvantage (NDI, Fig. 3d) or social vulnerability (for example, SoVI, Fig. 3e).

Our results are subject to several important limitations, uncertainties and caveats. First, major fluvial flood hazards simulated in this study are the result of levee and flood wall overtopping, which is sensitive to uncertainty in our estimates of 100-year flood peaks (Fig. 5 and Supplementary Table 5) and uncertainty in levee heights (~19.2 cm RMSE[45]). Combinations of lower peak flows and higher flood defenses would contribute to less overtopping, for example, and locations of overtopping are sensitive to local minima in levee heights (Supplementary Methods). Second, pluvial flood hazards may be overestimated in some areas because street runoff is assumed to reach secondary drainage pipes and channels by overland flow as opposed to subsurface drain pipes (Methods). On the other hand, fluvial hazards could be underestimated on the basis of the assumption of no levee or dam failures and no obstruction of channels by debris, which is at odds with the experiences of recent flood disasters such as Hurricane Katrina[46] and is a realistic concern based on dam risk ratings and levee inspection reports for Los Angeles (Supplementary Fig. 1). A likely range

of exposure is obtained by simulating the 100-year return event with each hazard driver evaluated the 5th and 95th percentile (Fig. 5 and Supplementary Table 1). Flood impacts could also be explored more deeply with measures such as expected losses, economic disruption, job losses, fatalities, injuries, human displacement and consequences for community cohesion, cultural heritage and social networks.

Yet the combination of high-resolution flood modelling and socioeconomic data reveals that flood risks within the densely populated Los Angeles region may be considerably underestimated—and that the greatest risks are borne disproportionately by Black and disadvantaged populations. Such inequities are probably reinforced by the challenges and costs of navigating the numerous federal and state agencies and local governments that provide resources for flood protection, which may be a substantial barrier to less affluent or marginalized communities. Our quantitative approach, which could be replicated for any US urban or rural region, thus highlights communities where flood risks are disproportionately large and provides critical data for more effective and equitable allocation of state and federal aid resources. Furthermore, integrated modelling of hazards and exposure as presented here offers an opening for dialogue among communities at risk of flooding, researchers and decision-makers in government (for example, ref. [47]), thereby enabling a more inclusive process of planning and projects to reduce the risks of future flood disasters (for example, ref. [48]). Replication elsewhere calls for acquiring and processing several urban datasets and local gauge records (Methods) and carrying out numerous checks for model accuracy and consistency, a manual process that can take an experienced modeller weeks to months. Nevertheless, the effort is likely to be far more cost-effective, time-sensitive and useful to marginalized communities than past practices in the United States of patching together reach-by-reach models of flood hazards[24].

Methods

Site description and parcel data

The study domain corresponds to the coastal plain of Los Angeles south of the Santa Monica Mountains. Data characterizing flood hazards, land use, lot area, property value, population, income, race, ethnicity, disadvantage and vulnerability were characterized across 1,767,588 land parcels to enable regional- and municipal-scale exposure analysis. Land parcels represent the smallest unit of land for the purpose of ownership. Flood hazard, land use, lot area and property values were resolved for each parcel and all other variables were downscaled from 2020 US census data at the block-group and/or census-tract scale. Tracts are small, contiguous, relatively permanent statistical subdivisions of a county or area, which generally have population sizes 1,200–8,000 and optimally near 4,000 (ref. [49]). Block groups are divisions of the same census tract, generally containing 600–3,000 people.

Parcel shapefiles with lot area, land use and assessor's value were accessed from the Los Angeles County Open Data Portal[31]. Population was estimated dasymetrically by apportioning the block-group population from the 2020 census across residential parcels in proportion to lot area[16] and zero population was ascribed to commercial or other parcel types. Each residential parcel was also assigned a non-Hispanic Black, Hispanic, non-Hispanic Asian and non-Hispanic White population fraction corresponding to the block-group fraction computed from census data. The study area population is 9,105,286 which by ethnicity is 48.2% Hispanic and by race is 49% White, 22.0% other, 14.2% Asian, 8.6% Black, 4.4% two or more races, 0.7% Native American and 0.3% Hawaii and other Pacific Islander.

Neighbourhood disadvantage index

NDI was developed from literatures on neighbourhood disadvantage, urban and concentrated poverty, neighbourhood effects and residential segregation (for example, refs. [50,51]). NDI was estimated at the block-group rather than census-tract level to enable a more precise understanding of social exposure in terms of exactly who is affected by flood hazards. The NDI closely follows recent sociological indices of neighbourhood disadvantage (for example, ref. [52]). The NDI incorporates 25 different indicators into one scale (Supplementary Table 3). The indicators were drawn from the 2019 5-year Census American Community Survey[32]. The unit of analysis is 216,498 block groups with valid data across the United States. The index is composed of measures across five domains: economic resources (for example, poverty and income), social policy (for example, access to welfare programmes), housing (for example, home ownership and rent burden), labour market (for example, unemployment rate) and demographics (single motherhood and educational attainment). All indicators and the NDI are signed such that higher values indicate greater disadvantage. The NDI is scaled to range from 0 to 1. The scale was constructed by using the standardized (mean 0, variance 1) values of the individual indicators and the scale reliability alpha was computed to be 0.92 using the Spearman–Brown Prophecy Formula[53]. Our analyses assign every land parcel within a block group the same NDI score. For the study area, 5th, 50th and 95th quantiles of NDI by land parcel are 0.27, 0.40 and 0.58, respectively.

The NDI includes many of the same indicators as earlier vulnerability indices including the social vulnerability index (SVI) developed by the Centers for Disease Control Agency for Toxic Substances and Disease Registry (CDC/ATSDR SVI)[54] and the SoVI developed at the University of South Carolina[55], with a few key exceptions (Supplementary Table 3). Unlike the CDC/ATSDR SVI and SoVI, we intentionally and purposefully chose to omit racial/ethnic minority status. We did so because including it problematically conflates indicators of disadvantage with causes of disadvantage. Having a high Black and Latino population share certainly may correlate with neighbourhood disadvantage but it is theoretically problematic to treat the presence of Black and Latino people as a disadvantage in itself. Also, unlike the CDC/ATSDR SVI, we omitted the measures of housing type and transportation (for example, mobile homes and multi-unit structures). Similarly, unlike SoVI, we omitted other infrastructure-related measures like hospitals per capita (measured at county level) and percentage housing units without a car. Although of course these certainly matter to vulnerability, we intentionally and strictly focused on socioeconomic disadvantage itself, not the physical environment and physical infrastructure in the neighbourhood. Finally, unlike previous indices, we omitted several demographic indicators that are only loosely related to disadvantage. For instance, we omitted the CDC/ATSDR SVI and SoVI measures of age structure (for example, percentage <5 or <17 or ≥65 years of age), the CDC measure of percentage with a disability and the SoVI measures of other demographics (for example, percentage females, median age, nursing home residents per capita, people per unit, female labour force participation and percentage employed in extractive or service industries). Supplementary Fig. 3 shows the distribution of NDI, SVI and SoVI for the United States and Los Angeles County.

The comparative analysis uses 67,864 census tracts across the United States and 1,955 tracts across Los Angeles County, for which SVI and SoVI data are jointly available from FEMA's National Risk Map[56]. Block-group resolution NDI values were averaged across each tract. For comparative purposes, each vulnerability index was normalized and tracts with NoData values were removed. US-wide, SVI exhibits the broadest distribution of vulnerability, centred on the median value of 0.5 and with an interquartile range between 0.37 and 0.64. SoVI and NDI have lower characterizations of vulnerability, exhibiting both lower median values and narrower interquartile ranges. All three distributions are minimally skewed, whereby SoVI exhibits the most skew of 0.78. For all three vulnerability indexes, the least vulnerable tracts (bottom 5th percentile) are marked by values around 0.2, while for the most vulnerable tracts (upper 5th percentile), the index range varies between 0.8 for SVI, 0.7 for NDI and 0.42 for SoVI. Compared to the United States as a whole, Los Angeles County median NDI and SVI values are ~18% higher, while the median SoVI value is nearly equal.

Compound flood hazard modelling

Flood hazard was estimated using the Parallel Raster Inundation Model (PRIMo) which solves the full shallow-water equations using

a dual-grid finite volume scheme that combines topographic data on a fine-grid with solution updates on a relatively coarse grid to overcome the computational bottlenecks of metropolitan-wide urban flood simulation[57]. Here, topography was resolved at 3 m resolution, shallow-water solution states were updated at 30 m resolution and depth was downscaled to 3 m resolution to estimate exposure. A 3 m resolution digital elevation model (DEM) was constructed mainly from two sources, 1/9th arcsec (3 m) USGS National Elevation Dataset (NED) DEM (primarily from 2016 lidar data[45]) for elevations >10 m and a 1 m resolution USGS topobathymetric DEM for elevations <10 m NAVD 88 including coastal bathymetry (data sources collected between 1930 and 2014; Supplementary Methods). The DEM was further subjected to several types of hydroconditioning for urban flood hazard modelling. First, channels in the land surface were 'burned' into the DEM to overcome line-of-site laser-scanning interference (for example, drainage channels that pass under roadways) and to approximate the capacity of culverts and subsurface gravity mains connecting open channels. These channels were aligned and sized with storm drain centerline and geometry data available from the County of Los Angeles[58]. Second, for roadway underpasses, the DEM was hydroconditioned to match the lower grade which is critical for flood water spreading through developed areas—otherwise underpasses are inaccurately modelled as blockage features. Data for roadway overpass locations were extracted from OpenStreetMap (https://www.openstreetmap.org/). Third, DEM heights representing major dams including Whittier Narrows Dam and Sepulveda Dam were buffered by 100 m to prevent artificial leakage flows arising from the PRIMo upscaling technique[53]. Fourth, a grid-edge classification technique was used to sharpen the representation of levees and flood walls[30]. With hydroconditioning of the DEM, the Los Angeles PRIMo model is configured to account for level 1 drainage infrastructure (dams/levees) and level 2 drainage infrastructure (secondary channels, culverts and drain pipes) but not level 3 drainage infrastructure (curb inlets and small storm pipes to nearest drainage channels). To model flow resistance, a 3 m resolution raster grid model of the Manning coefficient was developed on the basis of land use data available from OpenStreetMap and tabulated values of the Manning parameter for each land use category (Supplementary Table 4). The PRIMo model was configured to run using 756 tiles of raster grids of size 1,000 × 1,000, which corresponds to 756 million points.

PRIMo was configured to simulate pluvial, fluvial and coastal scenarios corresponding to 100-year return period events using different types of inputs. The pluvial scenario was configured by specifying a spatially distributed rainfall rate corresponding to the 100-year 24 h rainfall intensity defined by NOAA Atlas 14 (ref. [59]) and by simulating flood inundation for a period of 24 h which exceeds the time of concentration for the coastal plain (several hours). No infiltration was assumed because historical extreme flood events in the region (for example, 1861–62 and 1931) have been associated with several weeks of persistent rainfall that saturate the ground surface before episodes of extreme rainfall lasting hours[37]. The fluvial scenario was configured by specifying sources of water into primary and secondary flood channels to create flow rates representative of a 100-year return period streamflow event. The 100-year flow rate across the study area was estimated on the basis of frequency analysis of 51 different gauges maintained by the USGS, Los Angeles County and Orange County (Supplementary Table 5, Supplementary Fig. 1 and Supplementary Methods). Finally, the coastal scenario was developed by specifying a constant water level at the ocean boundary of PRIMo corresponding to the peak storm tide height with a 100-year return period based on water-level measurements at the Los Angeles NOAA tide gauge (9410660) and a period corresponding to 12 h. This accounts for the combined effects of tide and non-tide residuals but does not account for wave-driven flooding that occurs locally along the coast with the coincidence of high tides and long period swell. Hence, the coastal flood hazard assessment presented here is most representative within embayments sheltered from ocean waves (for example, Port of Los Angeles and Long Beach, Marina Del Ray) and may underestimate exposure along the open coast where wave transformation, runup and overtopping are drivers of coastal hazard (for example, Malibu). The 100-year return period value for each hazard driver (rainfall rate, streamflow and storm tide) was estimated at the 50th percentile to provide a most likely estimate of exposure for equity analysis and also at the 5th and 95th level to characterize uncertainty in exposure. Hazard drivers at the 5th and 95th percentile were estimated in the following ways: for the coastal hazard scenario, 5th and 95th percentile water surface elevations were extracted from the process-informed non-stationary extreme value analysis (ProNEVA) software package[60] executed using a 98-year block-maximum time series of observed ocean surface elevations at NOAA's Los Angeles tide gauge (NOAA 9410660); for the fluvial scenario, 5th and 95th percentile discharge values at each gauge location were extracted from HEC-SSP software (Supplementary Table 5); and for the pluvial scenario, 5th and 95th percentile spatially distributed depths were obtained from NOAA Atlas 14 as GIS grids[59]. PRIMo flood hazard simulations were performed in parallel over 756 compute cores on Cheyenne at the NCAR-Wyoming Supercomputing Center[57]. The model speed (ratio of simulation duration to wall clock time) for an upscale factor of 2 and 10 was 0.29 and 27.4, respectively. Flood hazard depth at 3 m spatial resolution was output from PRIMo for all three scenarios and a composite flood hazard distribution was also computed for the region on the basis of the pointwise maximum across the scenarios. Flood hazard at each land parcel was estimated on the basis of the average value across the area of the land parcel[61]. Model validation was approached with a combination of bottom-up exploration of model sensitivities and top-down assessment of the credibility of aggregated information (Supplementary Methods)[62].

Exposure and equity analysis

Exposed populations were computed by summing parcel-level population across parcels with a flood depth above a prescribed threshold (for example, 3, 10, 30 and 100 cm). Furthermore, populations by race and ethnicity were estimated by summing the product of parcel-level population and ethnic/racial fractions. Summations were performed at the County and local (municipal) scale on the basis of municipal tax rate affiliations for each parcel provided by Los Angeles County. FER is computed at the County scale and at the local (municipal) scale. In both cases, population fractions at the County scale are the basis for normalization (that is, fractions used in the denominator of the FER calculation) to frame representativeness by city in a regional context. Lorenz curves were developed at the County scale by sorting the parcel-level dataset in accordance with a specific factor (for example, property value per area) and then building cumulative distribution functions for population (for the x axis) and population-weighted flood hazard (for the y axis). Factors considered for sorting include non-Hispanic Black, Hispanic, non-Hispanic Asian and non-Hispanic White population fractions, property value per area, income, NDI and SoVI. All cumulative distribution functions were normalized by the maximum values so Lorenz curves scale from zero to unity on both axes. Furthermore, Gini coefficients are computed as indicators of inequality[34] and the fraction of the hazard associated with the upper half of the population is computed as a second indicator of inequality.

Reporting summary

Further information on research design is available in the Nature Research Reporting Summary linked to this article.

Data availability

The parcel-level dataset developed for this study is available through the Dryad and digital repository accessible at https://doi.org/10.7280/D1RH7Z.

Code availability

Codes used for exposure and equity analysis are available through the Zenodo digital repository accessible at https://doi.org/10.7280/D1RH7Z. Custom codes in Fortran, Matlab, Python and R used for data preparation, flood simulation and postprocessing are available upon written request from the authors.

References

1. Smith, A. B. *U.S. Billion-dollar Weather and Climate Disasters, 1980–Present* (NCEI, 2020); https://doi.org/10.25921/stkw-7w73
2. National Academies of Sciences, Engineering, and Medicine *Framing the Challenge of Urban Flooding in the United States* (National Academies Press, 2019).
3. Rainey, J. L., Brody, S. D., Galloway, G. E. & Highfield, W. E. Assessment of the growing threat of urban flooding: a case study of a national survey. *Urban Water J.* **18**, 375–381 (2021).
4. Gall, M., Borden, K. A., Emrich, C. T. & Cutter, S. L. The unsustainable trend of natural hazard losses in the United States. *Sustainability* **3**, 2157–2181 (2011).
5. Zhang, W., Villarini, G., Vecchi, G. A. & Smith, J. A. Urbanization exacerbated the rainfall and flooding caused by hurricane Harvey in Houston. *Nature* **563**, 384–388 (2018).
6. Davenport, F. V., Burke, M. & Diffenbaugh, N. S. Contribution of historical precipitation change to US flood damages. *Proc. Natl Acad. Sci. USA* **118**, e2017524118 (2021).
7. Hino, M. & Nance, E. Five ways to ensure flood-risk research helps the most vulnerable. *Nature* **595**, 27–29 (2021).
8. Bullard, R. D. & Wright, B. *The Wrong Complexion for Protection: How the Government Response to Disaster Endangers African American Communities* (New York Univ. Press, 2012).
9. Chambliss, S. E. et al. Local- and regional-scale racial and ethnic disparities in air pollution determined by long-term mobile monitoring. *Proc. Natl Acad. Sci. USA* **118**, e2109249118 (2021).
10. Chakraborty, J., Collins, T. W. & Grineski, S. E. Exploring the environmental justice implications of Hurricane Harvey flooding in Greater Houston, Texas. *Am. J. Public Health* **109**, 244–250 (2019).
11. Siders, A. R. & Keenan, J. M. Variables shaping coastal adaptation decisions to armor, nourish, and retreat in North Carolina. *Ocean Coast. Manag.* **183**, 105023 (2020).
12. Wing, O. E. J. et al. Inequitable patterns of US flood risk in the Anthropocene. *Nat. Clim. Change* **12**, 156–162 (2022).
13. Finch, C., Emrich, C. T. & Cutter, S. L. Disaster disparities and differential recovery in New Orleans. *Popul. Environ.* **31**, 179–202 (2010).
14. *WMO Atlas of Mortality and Economic Losses from Weather, Climate and Water Extremes (1970–2019)* (World Meteorological Organization, 2021).
15. Brakenridge, R. *Global Active Archive of Large Flood Events, 1985–Present* (Dartmouth Flood Observatory, 2021); https://floodobservatory.colorado.edu/Archives/index.html
16. Tate, E., Rahman, M. A., Emrich, C. T. & Sampson, C. C. Flood exposure and social vulnerability in the United States. *Nat. Hazards* **106**, 435–457 (2021).
17. Porter, K. et al. *Overview of the ARkStorm Scenario* (USGS, 2011); https://pubs.usgs.gov/of/2010/1312/
18. Ralph, F. M., Dettinger, M. D., Cairns, M. M., Galarneau, T. J. & Eylander, J. Defining "atmospheric river": how the glossary of meteorology helped resolve a debate. *Bull. Am. Meteorol. Soc.* **99**, 837–839 (2018).
19. Jones, L. M. *The Big Ones: How Natural Disasters have Shaped Us (and What we can do About Them)* (Anchor Books, 2019).
20. *Population Estimates for Los Angeles County for July 1, 2021* (U.S. Census Bureau, accessed 1 February 2022); https://www.census.gov/quickfacts/losangelescountycalifornia
21. *Regional Data, GDP and Personal Income for Los Angeles, CA* (U.S. Bureau of Economic Analysis, accessed 1 February 2022); https://apps.bea.gov/itable/iTable.cfm?ReqID=70&step=1&acrdn=5
22. Orsi, J. *Hazardous Metropolis: Flooding and Urban Ecology in Los Angeles* (Univ. of California Press, 2004).
23. Wing, O. E. J. et al. Validation of a 30 m resolution flood hazard model of the conterminous United States. *Water Resour. Res.* **53**, 7968–7986 (2017).
24. Bates, P. D. et al. Combined modeling of US fluvial, pluvial, and coastal flood hazard under current and future climates. *Water Res.* **57**, e2020WR028673 (2021).
25. Sheng, J. & Wilson, J. P. Watershed urbanization and changing flood behavior across the Los Angeles metropolitan region. *Nat. Hazards* **48**, 41–57 (2009).
26. *Hydraulics Report. Floodplain Analysis, Los Angeles River: Barham Boulevard to First Street. Flood Plain Management Services Special Study. Los Angeles, California* (U.S. Army Corps of Engineers, 2016); https://eng2.lacity.org/projects/LARIVER_Glendale_Narrows/docs/LAR_FPMS_Hydraulic_Report_FINAL_October2016_CompleteDocument.pdf
27. *Levee Certification Program* (Los Angeles County Department of Public Works, accessed 1 February 2022); https://dpw.lacounty.gov/wmd/nfip/dsp_LeveeCertificationFAQs.aspx
28. *Levee Safety Program. Inspection Summaries for the Los Angeles River, San Gabriel River, Rio Hondo Channel, and Compton Creek* (US Army Corps of Engineers, 2022); https://www.spl.usace.army.mil/Missions/Civil-Works/Levee-Safety-Program/
29. *Engineering and Design, Safety of Dams—Policy and Procedures* (US Army Corps of Engineers, 2011).
30. Kahl, D. T., Schubert, J. E., Jong-Levinger, A. & Sanders, B. F. Grid edge classification method to enhance levee resolution in dual-grid flood inundation models. *Adv. Water Res.* **168**, 104287 (2022).
31. *County of Los Angeles Open Data* (County of Los Angeles, accessed 1 February 2022); https://data.lacounty.gov/
32. *American Community Survey 5-Year Data (2009–2019): Detailed Tables* (U.S. Census Bureau, 2020); https://www.census.gov/data/developers/data-sets/acs-5year.html
33. Messager, M. L., Ettinger, A. K., Murphy-Williams, M. & Levin, P. S. Fine-scale assessment of inequities in inland flood vulnerability. *Appl. Geogr.* **133**, 102492 (2021).
34. Dorfman, R. A formula for the Gini coefficient. *Rev. Econ. Stat.* **61**, 146 (1979).
35. Mach, K. J. et al. Managed retreat through voluntary buyouts of flood-prone properties. *Sci. Adv.* **5**, eaax8995 (2019).
36. Lehmann, M., Major, D. C., Fitton, J. M., Doust, K. & O'Donoghue, S. Towards a typology for coastal towns and small cities for climate change adaptation planning. *Ocean Coast. Manag.* **212**, 105784 (2021).
37. Sanders, B. F. & Grant, S. B. Re-envisioning stormwater infrastructure for ultrahazardous flooding. *WIREs Water* **7**, e1414 (2020).
38. Markhvida, M., Walsh, B., Hallegatte, S. & Baker, J. Quantification of disaster impacts through household well-being losses. *Nat. Sustain.* **3**, 538–547 (2020).
39. Shi, L. From Progressive cities to resilient cities: lessons from history for new debates in equitable adaptation to climate change. *Urban Aff. Rev.* **57**, 1442–1479 (2021).
40. Domingue, S. J. & Emrich, C. T. Social vulnerability and procedural equity: exploring the distribution of disaster aid across counties in the United States. *Am. Rev. Public Admin.* **49**, 897–913 (2019).
41. Hornbeck, R. & Naidu, S. When the levee breaks: black migration and economic development in the American South. *Am. Econ. Rev.* **104**, 963–990 (2014).

42. Smiley, K. T. Social inequalities in flooding inside and outside of floodplains during Hurricane Harvey. *Environ. Res. Lett.* **15**, 0940b3 (2020).
43. Winsemius, H. C., Van Beek, L. P. H., Jongman, B., Ward, P. J. & Bouwman, A. A framework for global river flood risk assessments. *Hydrol. Earth Syst. Sci.* **17**, 1871–1892 (2013).
44. Bakkensen, L. & Barrage, L. *Flood Risk Belief Heterogeneity and Coastal Home Price Dynamics: Going Under Water?* (NBER, 2017); http://www.nber.org/papers/w23854.pdf; https://doi.org/10.3386/w23854
45. *2015–2016 LARIAC Lidar: Los Angeles Region, CA*. (OCM Partners, 2022); https://www.fisheries.noaa.gov/inport/item/55233
46. Galloway, G. E. Flood risk management in the United States and the impact of Hurricane Katrina. *Int. J. River Basin Manag.* **6**, 301–306 (2008).
47. Sanders, B. F. et al. Collaborative modeling with fine-resolution data enhances flood awareness, minimizes differences in flood perception, and produces actionable flood maps. *Earth's Future* **8**, 2019 (2020).
48. Goodrich, K. A. et al. Addressing pluvial flash flooding through community-based collaborative research in Tijuana, Mexico. *Water* **12**, 1257 (2020).
49. *Glossary* (U.S. Census Bureau, 2022); https://www.census.gov/programs-surveys/geography/about/glossary.html
50. Carpiano, R. M. Neighborhood social capital and adult health: an empirical test of a Bourdieu-based model. *Health Place* **13**, 639–655 (2007).
51. Sampson, R. J., Raudenbush, S. W. & Earls, F. Neighborhoods and violent crime: a multilevel study of collective efficacy. *Science* **277**, 918–924 (1997).
52. Wodtke, G. T., Elwert, F. & Harding, D. J. Neighborhood effect heterogeneity by family income and developmental period. *Am. J. Sociol.* **121**, 1168–1222 (2016).
53. *Stata: Release 17 Multivariate Statistics Reference Manual* (StataCorp, 2021).
54. *The CDC/ATSDR Social Vulnerability Index (CDC/ATSDR SVI)* (The Center for Disease Control and Agency for Toxic Substances and Disease Registry, accessed 1 February 2022); https://www.atsdr.cdc.gov/placeandhealth/svi/index.html
55. *The Social Vulnerability Index (SoVI) 2010–2014* (The University of South Carolina Hazards and Vulnerability Research Institute, accessed 1 February 2022); https://www.sc.edu/study/colleges_schools/artsandsciences/centers_and_institutes/hvri/data_and_resources/sovi/index.php
56. Zuzak, C. et al. The national risk index: establishing a nationwide baseline for natural hazard risk in the US. *Nat. Hazards* https://doi.org/10.1007/s11069-022-05474-w (2022).
57. Sanders, B. F. & Schubert, J. E. PRIMo: parallel raster inundation model. *Adv. Water Resour.* **126**, 79–95 (2019).
58. *Los Angeles County Storm Drain* (Los Angeles County Public Works, accessed 1 February 2022); https://pw.lacounty.gov/fcd/StormDrain/index.cfm
59. Perica, S. et al. *Precipitation-Frequency Atlas of the United States, California* NOAA Atlas 14 Vol. 6 v.2.3 (NOAA, 2014).
60. Ragno, E., AghaKouchak, A., Cheng, L. & Sadegh, M. A generalized framework for process-informed nonstationary extreme value analysis. *Adv. Water Res.* **130**, 270–282 (2019).
61. Moftakhari, H., Schubert, J. E., AghaKouchak, A., Matthew, R. A. & Sanders, B. F. Linking statistical and hydrodynamic modeling for compound flood hazard assessment in tidal channels and estuaries. *Adv. Water Resour.* **128**, 28–38 (2019).
62. Sayers, P. et al. Believe it or not? The challenge of validating large scale probabilistic risk models. *E3S Web Conf.* **7**, 11004 (2016).
63. *World Terrain Base* (ESRI, 2022); https://www.arcgis.com/home/item.html?id=33064a20de0c48d2bb61efa8faca93a8

Acknowledgements

We express our thanks to the County of Los Angeles and the County of Orange for assistance with access to data used for this study. We thank S. Grant for valuable discussion and A. Jong-Levinger for assistance preparing model data. We also acknowledge high-performance computing support from the NCAR-Wyoming Supercomputing Center provided by the National Science Foundation and the State of Wyoming and supported by NCAR's Computational and Information Systems Laboratory. Figures with maps were created using ArcGIS software by Esri. This work was supported by grants from the National Science Foundation (Coastlines and People grant no. ICER-1940171, INFEWS grant no. EAR-1639318 and grant no. HDBE-2031535), the NOAA Effects of Sea Level Rise Program (grant no. NA16NOS4780206) and the Ridge to Reef NSF Research Traineeship (grant no. DGE-1735040).

Author contributions

The project concept was conceived by A.A., D.B., S.J.D., F.F., K.J.M., R.A.M., B.F.S., J.E.S. and N.U. who also contributed to funding acquisition. The methodology was developed and validated by D.B., S.J.D., D.K., B.F.S. and J.E.S. The investigation and formal analysis was by S.J.D., K.J.M., B.F.S. and J.E.S. The original draft was prepared by D.B., S.J.D., K.J.M, B.F.S. and J.E.S. All authors contributed to review and editing.

Competing interests

The authors declare no competing interests.

Additional information

Supplementary information The online version contains supplementary material available at https://doi.org/10.1038/s41893-022-00977-7.

Correspondence and requests for materials should be addressed to Brett F. Sanders.

Peer review information *Nature Sustainability* thanks Paul Bates, Oronde Drakes and Mathis Messager for their contribution to the peer review of this work.

nature research

Corresponding author(s): Brett F. Sanders

Last updated by author(s): Aug 31, 2022

Reporting Summary

Nature Research wishes to improve the reproducibility of the work that we publish. This form provides structure for consistency and transparency in reporting. For further information on Nature Research policies, see our Editorial Policies and the Editorial Policy Checklist.

Statistics

For all statistical analyses, confirm that the following items are present in the figure legend, table legend, main text, or Methods section.

n/a	Confirmed
☒	☐ The exact sample size (*n*) for each experimental group/condition, given as a discrete number and unit of measurement
☒	☐ A statement on whether measurements were taken from distinct samples or whether the same sample was measured repeatedly
☒	☐ The statistical test(s) used AND whether they are one- or two-sided *Only common tests should be described solely by name; describe more complex techniques in the Methods section.*
☒	☐ A description of all covariates tested
☒	☐ A description of any assumptions or corrections, such as tests of normality and adjustment for multiple comparisons
☒	☐ A full description of the statistical parameters including central tendency (e.g. means) or other basic estimates (e.g. regression coefficient) AND variation (e.g. standard deviation) or associated estimates of uncertainty (e.g. confidence intervals)
☒	☐ For null hypothesis testing, the test statistic (e.g. *F*, *t*, *r*) with confidence intervals, effect sizes, degrees of freedom and *P* value noted *Give P values as exact values whenever suitable.*
☒	☐ For Bayesian analysis, information on the choice of priors and Markov chain Monte Carlo settings
☒	☐ For hierarchical and complex designs, identification of the appropriate level for tests and full reporting of outcomes
☒	☐ Estimates of effect sizes (e.g. Cohen's *d*, Pearson's *r*), indicating how they were calculated

Our web collection on statistics for biologists contains articles on many of the points above.

Software and code

Policy information about availability of computer code

Data collection	Scripts (custom codes) in Python (3.7) and Stata (16.0) were used to access the American Community Survey (ACS) data and calculate the Census block group resolution Neighborhood Disadvantage Index (NDI). Python (3.7) and ArcGIS Pro (2.9.0) were used to process and prepare spatial datasets including hydroconditioned topographic data and resistance parameter data based on landcover/landuse data. Parcel level flood hazard data was estimated using the Parallel Raster Inundation Model (PRIMo) which is a custom code in Fortran maintained by the UCI Flood Lab with methods reported by Sanders and Schubert (Advances in Water Resources, 2019). Flood peaks required to generate fluvial flood hazard data were estimated using the Hydraulic Engineering Center Statistical Software Package (HEC-SSP 2.2). ArcGIS Pro (2.9.0) and Matlab (R2021a) were used to prepare a table of parcel-level flood risk.
Data analysis	Analysis of exposure regionally and at municipal levels [including estimates of inequities (Lorenz curves, flood exposure representativeness)] was performed using scripts (custom codes) in Matlab (R2021a). Spatial mapping was carried out using ArcGIS Pro (2.9.0).

For manuscripts utilizing custom algorithms or software that are central to the research but not yet described in published literature, software must be made available to editors and reviewers. We strongly encourage code deposition in a community repository (e.g. GitHub). See the Nature Research guidelines for submitting code & software for further information.

Data

Policy information about availability of data

All manuscripts must include a data availability statement. This statement should provide the following information, where applicable:

- Accession codes, unique identifiers, or web links for publicly available datasets
- A list of figures that have associated raw data
- A description of any restrictions on data availability

The parcel level dataset developed for this study is available
through the Dryad digital repository accessible at https://doi.org/10.7280/D1RH7Z

Field-specific reporting

Please select the one below that is the best fit for your research. If you are not sure, read the appropriate sections before making your selection.

☐ Life sciences ☐ Behavioural & social sciences ☒ Ecological, evolutionary & environmental sciences

For a reference copy of the document with all sections, see nature.com/documents/nr-reporting-summary-flat.pdf

Ecological, evolutionary & environmental sciences study design

All studies must disclose on these points even when the disclosure is negative.

Study description	This study involved the development of a land parcel dataset for Los Angeles County, California, USA containing information about flood hazards, population, racial and ethnic population fractions, property value, land cover/land use, and neighborhood disadvantage and social vulnerability.
Research sample	NA. The analysis did not involve sampling the county-wide dataset.
Sampling strategy	NA
Data collection	Primary data are obtained from publicly accessible sources: Parcel shape files with lot area, land use, and Assessor's value are accessed from the Los Angeles County Open Data portal. Population and demographic information is obtained from US Census and American Community Survey Datasets. The census tract scale Social Vulnerability Index (SoVI) and the CDC/ATSDR Social Vulnerability Index (SVI) were accessed from online sources. Gage records of annual maximum streamflow were obtained from the Public Works departments of Los Angeles and Orange County . Digital topographic data for flood hazard modeling of Los Angeles and Orange County was obtained from USGS and NOAA.
Timing and spatial scale	NA
Data exclusions	None.
Reproducibility	Based on a rigorous validation process and treatment of uncertainty, we are confident that our estimates of exposure and findings about inequalities are robust. We emphasize that several echnical reports document that major flood channels in the region including the upper LA River, Dominguez Channel, and Compton Creek are no longer able to contain a 100 year flood flow - as documented in the paper. Hence, our modeling of overtopping is consistent with numerous technical studies of channel capacity.
Randomization	NA
Blinding	NA

Did the study involve field work? ☐ Yes ☒ No

Reporting for specific materials, systems and methods

We require information from authors about some types of materials, experimental systems and methods used in many studies. Here, indicate whether each material, system or method listed is relevant to your study. If you are not sure if a list item applies to your research, read the appropriate section before selecting a response.

Materials & experimental systems

n/a	Involved in the study
☒	☐ Antibodies
☒	☐ Eukaryotic cell lines
☒	☐ Palaeontology and archaeology
☒	☐ Animals and other organisms
☒	☐ Human research participants
☒	☐ Clinical data
☒	☐ Dual use research of concern

Methods

n/a	Involved in the study
☒	☐ ChIP-seq
☒	☐ Flow cytometry
☒	☐ MRI-based neuroimaging